PAPER

SERS-active substrate assembled by Ag NW-embedded porous polystyrene fibers†

Shulin Chen,‡[ab] Chen Ding,‡[b] Yong Lin,[b] Xinzhou Wu,[b] Wei Yuan, [iD] *[b] Xiuqing Meng,*[a] Wenming Su [iD] [b] and Ke-Qin Zhang [iD] *[c]

Here we demonstrate a novel SERS-active substrate assembled by silver nanowire (Ag NW)-embedded porous polystyrene (PS) fibers. Ag NWs are synthesized through a glycerol-mediated solvothermal method firstly, then electrospun into PS porous fibers. The as-synthesized Ag NWs are embedded in PS fiber and aligned orderly along the axial direction. Porous structure appears in PS fiber due to the phase separation induced by rapid evaporation of solvents. Large amounts of holes not only greatly improve the sample collection efficiency of the SERS-active substrate, but also significantly facilitate the adsorption of target molecules on the surface of Ag NWs, thus increasing the probability of enhancement of target molecules. In addition, compared with polyvinyl alcohol (PVA) and polyvinyl pyrrolidone (PVP), PS has better solvent resistance. The detection limit of 4-aminothiophenol (4-ATP) on our fabricated electrospun fiber mats is 10^{-7} M, and the electrospun fiber mats showed good reproducibility of SERS signal detection. This study proposes a feasible strategy for the large-scale preparation of flexible SERS-active substrate assembled by Ag NW-embedded porous PS fibers. The produced flexible SERS substrates may have potential application in wearable sensors for the trace detection of chemical and biological molecules.

1. Introduction

Surface-enhanced Raman scattering (SERS) mainly utilizes the greatly enhanced electromagnetic (EM) field as well as the localized surface plasmon resonances generated on metal surfaces to obtain the enhanced Raman signal of a target molecule.[1,2] As a spectroscopic analysis technique, SERS shows great capability for the trace detection of chemical and biological molecules at a very low concentration, even to the single-molecule level, and has potential applications in the fields of biochemical sensing, environmental monitoring, food security and biomedical analysis.[3–6] Since the discovery of SERS in the 1970s, significant progress has been made in the fabrication of sensitive and active SERS substrates. To date, various SERS-active substrates modified with different enhancement materials have been prepared, including roughened metal substrates,[7] noble metal nanostructure assemblies,[8] a small number of semiconductor[9] and metal oxides,[10] and even graphene.[11] In addition to the substrate surface modification, some metal nanomaterials are directly sprayed onto analyte samples to realize Raman enhancement.[12,13]

Recently, more and more efforts have been employed to explore the flexible SERS-active substrates. Compared with traditional rigid metal substrates, flexible SERS-active substrates can attach to the surface of human skin or irregularly shaped objects to realize the *in situ* and real-time measurement of analytes. Therefore, the flexible SERS-active substrate is regarded as a promising candidate for the next generation of wearable and portable sensing devices.[14–17]

Among the various flexible substrates, electrospun polymer nanofibers have been shown to be one of the most promising templates to pack noble metal nanostructures with great precision due to their advantages of high mechanical flexibility, large specific surface and good permeability.[18] Table S1† summarizes the recently reported papers on flexible SERS substrates based on metallic nanomaterials and electrospun polymer fibers. Many polymers, such as polyvinyl alcohol (PVA),[19] polyvinyl pyrrolidone (PVP),[20] polyacrylic acid (PAA),[21] poly(ε-caprolactone) (PCL),[22] polyacrylonitrile (PAN)[23] and poly(ʟ-lactic acid) (PLLA),[24] have been utilized to combine with different Au and Ag nanostructures to fabricate various flexible substrates for SERS.[15,25,26] In general, there are two different

ᵃZhejiang Provincial Key Laboratory of Solid State Optoelectronic Devices, Zhejiang Normal University, Jinhua 321004, China. E-mail: xqmeng@zjnu.cn

ᵇPrintable Electronics Research Centre, Suzhou Institute of Nano-tech and Nano-bionics, Chinese Academy of Sciences, Suzhou 215123, China. E-mail: wyuan2014@sinano.ac.cn

ᶜNational Engineering Laboratory for Modern Silk, College of Textile and Clothing Engineering, Soochow University, Suzhou 215123, China. E-mail: kqzhang@suda.edu.cn

† Electronic supplementary information (ESI) available: Photograph of the synthesized Ag NWs in flask; diameter distribution of electrospun Ag NWs/PS composite fibers; number of Ag NWs in electrospun fiber as faction of Ag NWs content in electrospun solutions; surface and cross-section SEM images of Ag NWs/PS solid composite fiber; transport of FITC/ethanol solution in Ag NWs/PS porous and solid composite films. See DOI: 10.1039/d0ra01454k

‡ These authors contributed equally to this work.

composite modes for metal nanomaterials and electrospun fibers: one is embedding into the fiber by directly electrospinning the pre-mixed polymer solution, and the other is immobilization on the fiber surface by surface modification or *in situ* synthesis.[23,24] It is obvious from Table S1† that the electrospun fiber substrates with metal nanoparticles immobilized onto the fiber surface have lower detection limit and higher enhancement factor than the electrospun substrates with metal nanoparticles embedded into the fibers. However, these exposed metal nanoparticles are vulnerable to water vapor oxidation and mechanical damage, which seriously weakens the enhancement effect for SERS substrates.[22,27] For the embedded mode of metal nanoparticle or nanowires, it is true that the polymer outside the metal nanomaterials can protect them from contamination and surface oxidation, especially for Ag nanostructures, which gives the composite a long lifetime.[17] However, the encapsulated polymer also prevents the target molecules from adsorbing on the surface of metal nanostructures quickly and accurately, which will seriously reduce the efficiency of sample collection. Therefore, in this work, we designed a new SERS substrate based on electrospun fibers, which not can only protect the metal nanomaterials from oxidation and mechanical damage, but also enable the target molecules to easily access the enhancement region and significantly improve the collection efficiency of target samples. Furthermore, PVA and PVP are popular polymer materials for electrospinning, and they are usually used as supporting materials for metal nanostructures for SERS (see in Table S1†). Nevertheless, these biocompatible polymers are water soluble, which greatly limits the applications of these metal/nanofiber composites as SERS-active substrates because these polymer host matrixes have weak resistance to some common and green solvents, such as ethanol or water.

Herein, we describe a novel SERS-active substrate assembled by Ag NW-embedded porous PS fibers. Highly SERS-active Ag NWs are synthesized firstly and then electrospun into PS porous fibers. During the process of electrospinning, as-synthesized Ag NWs are embedded in PS fiber and aligned along the axial direction; at the same time, an interconnected porous structure appears in the PS fiber due to the phase separation induced by rapid evaporation of solvents.[28–30] The formation of pore structures not only greatly improves the sample collection efficiency of SERS-active substrate but also significantly facilitates the adsorption of target molecules on the surface of Ag NWs, thus increasing the enhancement probability of target molecules. In addition, compared with PVA and PVP, PS has better solvent resistance. This study proposes a feasible strategy for the large-scale preparation of flexible SERS-active substrate assembled by Ag NW-embedded porous PS fibers. The produced flexible SERS substrates may have potential application in wearable sensors for the trace detection of chemical and biological molecules.

2. Experimental section

2.1 Materials

PS was bought from Wen'an Kanngda plastics factory; PVP (M_w: 58 000, Aladdin Chemistry Co. Ltd), 4-aminothiophenol (4-ATP,

Aldrich, ≥97%, Macklin Biochemical Co. Ltd), sodium chloride (NaCl, AR), glycerol (AR), tetrahydrofuran (THF, AR), ethanol (AR) and methanol (AR) were bought from Sinopharm Chemical reagent Co. Ltd; *N*,*N*-dimethylformamide (DMF, AR) from Jiangsu Qiangsheng Function Chemical Co. Ltd; $AgNO_3$ from Shanghai Chemical Reagent Co. Ltd.; fluorescein isothiocyanate (FITC ≥95%) from Shanghai Gold Wheat Co. Ltd. All materials and chemicals were used without further purification. Ultrapure water was used in all experiments.

2.2 Synthesis of Ag NWs

Ag NWs were synthesized through a glycerol-mediated solvothermal method, as reported by Yu's group.[31] Briefly, 10^{-4} mol PVP was added into 190 ml glycerol with stirring (80 rpm) and heated at 90 °C until the PVP was dissolved completely. After the solution temperature cooled to room temperature, 0.01 mol $AgNO_3$ powder was added into the solution. Then, the pre-prepared 10 ml glycerol solution containing 10^{-3} mol NaCl and 0.5 ml H_2O was poured into the reaction flask. The solution temperature was raised from room temperature to 210 °C in about 20 minutes with gentle stirring (50 rpm). Once the temperature reached 210 °C, the heating was stopped, and the solution temperature was cooled to room temperature naturally. A solution with grey colour (see in Fig. S1†) was obtained and transferred to a beaker, and an equal amount of ultrapure water was added. In order to remove PVP and rare Ag nanoparticles, the final solution was stabilized for 5–7 days and then washed with ethanol twice with the aid of a centrifuge (8000 rpm, 5 min). Finally, the Ag NWs were dispersed in ethanol at the concentration of 250 mg ml^{-1}, and the solution was preserved in a 4 °C refrigerator.

2.3 Preparation of Ag NWs/PS mixed solution

Firstly, the as-prepared Ag NW–ethanol dispersion was diluted to 10 mg ml^{-1} with ethanol. Then, four Ag NW–ethanol solutions, 1 ml (10 mg), 2.5 ml (25 mg), 3.5 ml (35 mg), and 5.0 ml (50 mg), were centrifuged to remove the upper ethanol solvents, respectively, and then the deposited Ag NWs were re-dispersed in DMF solution (7.2 g). The obtained four Ag NWs–DMF dispersions were transferred to four beakers and stirred for 20 minutes. Finally, 1.8 g PS slices, in quadruplicate, were added to the four beakers and stirred until PS slices were dissolved fully. Because the content of PS and DMF in the four solutions were the same, for convenience, the electrospun solutions were named according to the content of Ag NWs as 10 mg-Ag NWs/PS, 25 mg-Ag NWs/PS, 35 mg-Ag NWs/PS and 50 mg-Ag NWs/PS, respectively. 10 mg-Ag NWs/PVP and Ag NWs/PS/THF electrospun solutions were prepared just like the Ag NWs/PS/DMF electrospun solution.

2.4 Fabrication of Ag NWs/PS composite fibers

As shown in Fig. 1a, the prepared Ag NWs/PS mixed solutions were loaded into a 5 ml glass syringe connected with a metal needle of 0.5 mm inner diameter. The syringe was fixed horizontally onto a syringe pump (LSP02-1B, Baoding Longer Precision Pump Co., Ltd., China) with flow rate of 2 ml h^{-1}. A

high voltage (7 kV) was applied between the metallic needle and collector by a power supply (DW-P303-1AC, Tianjin Dongwen High Voltage Co., China). A grounded copper plate, used as a fiber collector, was positioned at the distance of 10 cm from the tip of the metallic needle. Temperature and humidity were controlled at 25 °C and 50%. All electrospun fiber mats were collected for 20 min unless otherwise specified.

2.5 Fabrication of Ag NWs/PS composite films

The composite porous film was prepared by spin-coating 50 mg-Ag NWs/PS/DMF mixture at 1000 rpm for 1 min. The composite solid film was produced by casting 50 mg-Ag NWs/PS/THF mixture on the slide and drying at room temperature for 3 hours.

2.6 Preparation of SERS samples

To prepare the SERS substrates, as-prepared Ag NWs/PS composites (electrospun fiber mats and casted films) were cut into small strips (1.0×0.5 cm^2). These strips were immersed into 4-aminothiophenol (4-ATP) solution (0.2 ml) with different concentrations for only 10 seconds, then these infiltrated strips were taken out quickly and dried at room temperature for 2 hours.

2.7 Characterization

The morphology of the synthesized Ag NWs and electrospun Ag NWs/PS porous fibers was observed by scanning electron microscopy (SEM, Hitachi S-4800). The alignment of Ag NWs in the PS fiber was examined by transmission electron microscopy (TEM, Tecnai G2 F20 S-Twin, operated at 200 kV). X-ray diffraction (XRD) patterns were collected by a Philips X'Pert-Pro MRD diffractometer with Cu kα radiation. The UV-Vis absorption spectrum of the Ag NWs–ethanol dispersion was measured by ultraviolet-visible-near infrared spectrophotometer (Lambda750, PerkinElmer). Fluorescent microscope images were taken using an upright fluorescence microscope (BX51W1, Olympus). Raman scattering spectra were recorded with a LabRam HR 800 spectrometer using the 532 nm line of semiconductor laser for excitation, with a power no more than 2 mW on the sample to prevent any damage to the samples; exposure time was 10 s and accumulation time was 5. All the optical pictures were taken using a Nikon D750 digital camera.

3. Results and discussion

Fig. 1a shows the fabrication process of Ag NWs/PS composite porous fiber *via* electrospinning technique. Electrospinning is an easy and high-throughput method to fabricate polymer fibers with a range of diameter from tens of nanometers to hundreds of micrometers.[18,32–34] During the drawing process of Ag NWs/PS mixed solution under high-voltage electrostatic field, the fluid jet is thermodynamically unstable due to solvent evaporation and moisture in the surrounding environment. The formation of pores in fibers can be explained by the competition between phase separation and solidification of the fluid jet during electrospinning. Usually, the phase separation is induced by solvent evaporation and vapor precipitation within the fluid jet, which constitutes the thermally induced phase separation and the vapor-induced liquid–liquid phase separation.[28–30] Finally, Ag NWs are embedded in the porous PS fiber and aligned along the axial direction. The porous structure greatly increases the capacity for sample adsorption, thus improving the efficiency of sample collection. On the other hand, because of the porous structure of PS fiber, the target molecules can access the region where the silver nanowires are not wrapped by the polymer quickly and accurately from these holes. As shown in Fig. 1b, the orientation of AgNWs can be well limited by the electrospun fiber template. When the NWs are contiguous to each other, hot spots appear, and the intensities of the Raman signals are enhanced, which facilitates SERS measurement.[20,35]

Ag NWs were synthesized with reference to the existing reports of Yu's group.[31] As shown in Fig. 2a, it is a high-throughput method, and the synthesized Ag NWs–ethanol dispersion presents a uniform grey colour. A typical SEM image (Fig. 2b) shows the synthesized Ag NWs have a high aspect ratio, with 70–130 nm diameter and 10–20 μm length. The XRD pattern in Fig. 2c confirms that the synthesized Ag NWs are
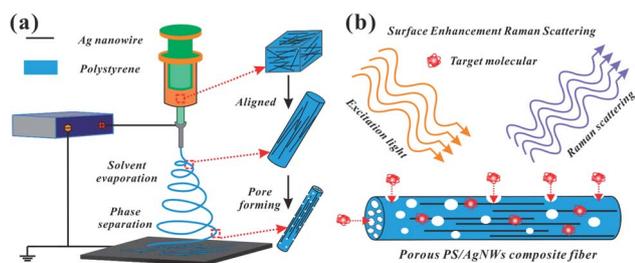

Fig. 2 (a) Photograph of synthesized Ag NW–ethanol dispersion; (b) SEM image of synthesized Ag NWs, (c) typical XRD pattern of synthesized Ag NWs, (d) UV-Vis absorption spectrum of Ag NWs–ethanol dispersion.

Fig. 1 Schematic illustration of (a) Ag NWs/PS composite porous fiber preparation process and (b) target molecules permeating into the surface of Ag NWs from the holes for SERS testing.
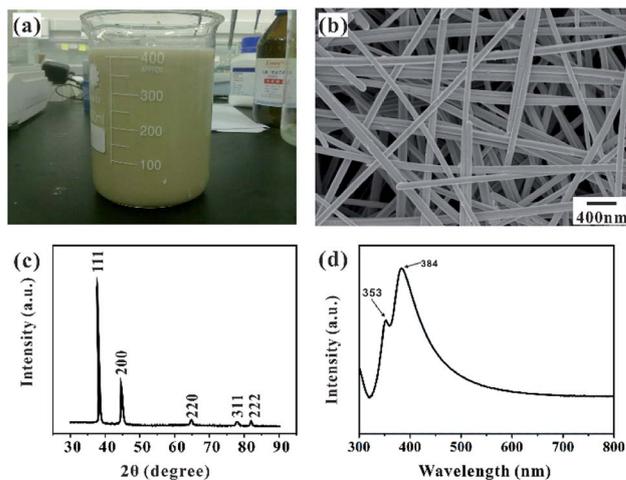
highly crystalline and exist purely in a face-centered cubic (FCC) structure.[16,20] Furthermore, the UV-Vis absorption spectrum of the Ag NWs–ethanol dispersion (Fig. 2d) displays typical two surface plasmon resonance (SPR) peaks at 353 and 384 nm. The SPR peak at 384 nm corresponds to the transverse plasmon resonance of nanowires,[36] and the weaker peak at 353 nm is attributable to the quadrupole resonance excitation of nanowires.[37,38]

Fig. 3a shows the prepared electrospun fiber mat with a large area of 10×10 cm^2. The disordered fibers were stacked on the collector to form a nonwoven mat, whose thickness depends on the electrospinning time, as shown in Fig. S2.† Compared with the pure PS fiber mat, the Ag NWs/PS composite fiber mat is more fluffy with the same electrospinning time. The thickness of the composite fiber mat collected for 20 min is about 400 μm, which is enough for the subsequent SERS experiments. The obtained Ag NWs/PS composite fiber mat presents uniform yellowish-brown color, which is similar to the color of the electrospun solution (inset picture in Fig. 3a). The typical SEM image in Fig. 3b shows that the composite fibers have uniform shape and size. The diameter distribution (Fig. S3†), measured through the statistics of SEM images by ImageJ, confirms that the fibers have a uniform diameter of 2.06 ± 0.25 μm. The surface and cross-sectional morphology of the composite fiber were observed using SEM. As we expected, there are large amounts of holes on the surface and inside of the composite fiber (Fig. 3c). The inset shows direct evidence that Ag NWs are embedded into the porous PS fibers. Observing by SEM, there are few Ag NWs on the fiber surface, which means most of the Ag NWs are embedded inside the matrix. Through distorting and stretching the composite fibers, Ag NWs come out of the broken fibers, as shown in Fig. 3d. In addition, the UV-Vis absorption spectrum of the Ag NWs/PS composite fiber mat was measured as shown in Fig. S4,† which indicates an obvious SPR peak at 359 nm.
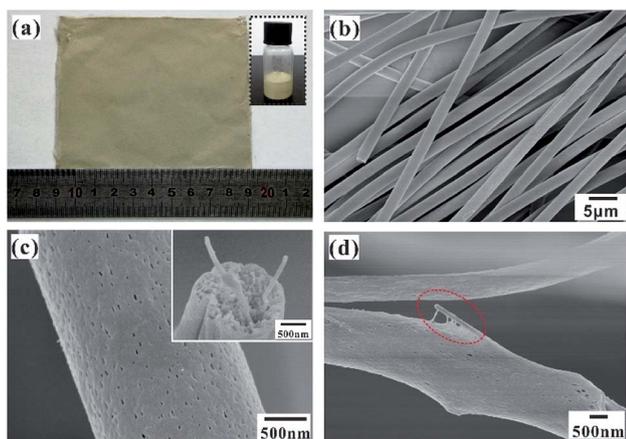
Fig. 4a shows a photograph of the electrospun fiber mats with different contents of Ag NWs. From left to right, the Ag NWs content are 10 mg, 25 mg, 35 mg and 50 mg, respectively. It is obvious that greater the content of Ag NWs, the deeper the color of the electrospun mat is. Furthermore, the electrospun Ag NWs/PS composite fiber was observed by TEM, as shown in Fig. 4b–e. From these images, we can clearly see that the Ag NWs are embedded in the PS matrix and arranged parallel to each other along the length of the fibers. When the Ag NW content is 10 mg (Ag NWs : PS : DMF = 10 mg : 1.8 g : 7.2 g), only one or two discontinuous nanowires are assembled within a single fiber (Fig. 4b). With increasing content of Ag NWs in the electrospun solution, more nanowires were embedded in PS fibers (Fig. S5†). By increasing the Ag NW content to 50 mg (Ag NWs : S : DMF = 50 mg : 1.8 g : 7.2 g), there are about eight nanowires assembled within one single fiber (Fig. 4e). It is true that the more Ag NWs in the fiber, the more "hot spots" it can provide for SERS effect.[20] However, if the amount of Ag NWs is further increased, the viscosity of the electrospun solution will be too high to spin fibers.

The solvent resistance of the host matrix for metal nanostructures is very important for practical SERS application. The existing literature reports that PVA and PVP are popular polymer materials for electrospinning, and they are usually used as supporting materials for metal nanostructures. However, these polymers have weak resistance to some common and green solvents, such as ethanol or water. As shown in Fig. 5, once immersed into ethanol and water, PVP-based fiber mats dissolve instantly, while PS-based fiber mats can stably exist in ethanol and water. Obviously, the poor solvent resistance of the

Fig. 3 (a) Photograph of electrospun 50 mg-Ag NWs/PS fiber mat (10×10 cm^2); inset is a photograph of the corresponding Ag NWs/PS/DMF mixed solution; (b) SEM image of Ag NWs/PS composite fibers; (c) magnified SEM images of surface and cross-section (inset) of a single composite fiber; (d) SEM image of Ag NWs exposed from a distorted composite fiber.
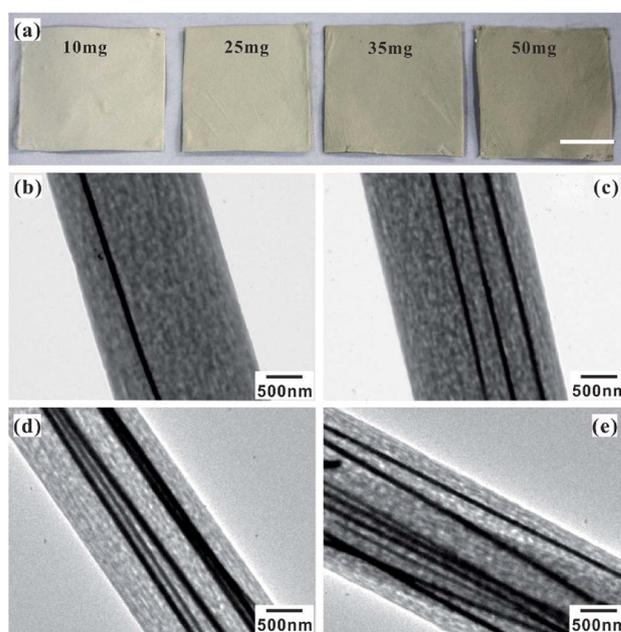

Fig. 4 (a) Photograph of the electrospun mats with different contents of Ag NWs, the scale bar is 5 cm; TEM images of Ag NWs/PS composite fibers with Ag NW content of (b) 10 mg, (c) 25 mg, (d) 35 mg and (e) 50 mg.

Paper

polymer matrix will greatly limit the application scenarios of these composite fibers for SERS. However, because of the chemically hydrophobic nature of PS polymer,[28,30] the water contact angle of the composite fiber mat is larger than 120°, as shown in Fig. S6,† which means that the obtained Ag NWs/PS fiber mat is not suitable for the collection and detection of molecules in aqueous solution, but it can still detect probe molecules in alcohol solution.

In order to understand the sample collection process of the Ag NWs/PS porous composite fiber, we conducted a penetration experiment with fluorescent solution (0.1 mol FITC in 10 ml ethanol). The detailed experimental process is briefly described as follows: firstly, a single porous fiber and a single solid fiber were respectively fixed on a glass substrate. Secondly, the FITC solution was dropped on one end of the porous fiber and the solid fiber, respectively, as shown in the inset of Fig. 6. Thirdly, the optical (Fig. 6a and c) and fluorescent (Fig. 6b and d) images were captured by laser confocal microscope. It should be noted that all the images were taken immediately after dropping the FITC solution on the end of the fibers. Obviously, the fluorescence solution permeated into the holes of the composite fiber quickly and was transported along the fiber's longitudinal direction (Fig. 6b), which confirms that target molecules can easily access the surface of Ag NWs. For comparison, the Ag NWs/PS solid composite fibers (Fig. S7†) were also fabricated by electrospinning of Ag NWs/PS/THF mixed solution (10 mg Ag NWs, 1.8 g PS, 7.2 g THF). As expected, the FITC/ethanol solution did not permeate the solid fiber at all (Fig. 6d). In addition to the fibers, the Ag NWs/PS porous and solid composite films were also prepared by spin-coating, shown in Fig. S8.† As expected, the fluorescent solution is unable to permeate the solid film, while the porous film showed a similar solution permeation phenomenon as porous fibers. These results reveal that porous structure greatly improves the sample collection efficiency of the SERS-active substrate and facilitates the adsorption of target molecules on the surface of Ag NWs.

The prepared Ag NWs/PS porous fibers can be used as SERS substrates. Herein, we used 4-ATP as the probe molecule for the SERS measurement to study the enhancement effects of the Ag
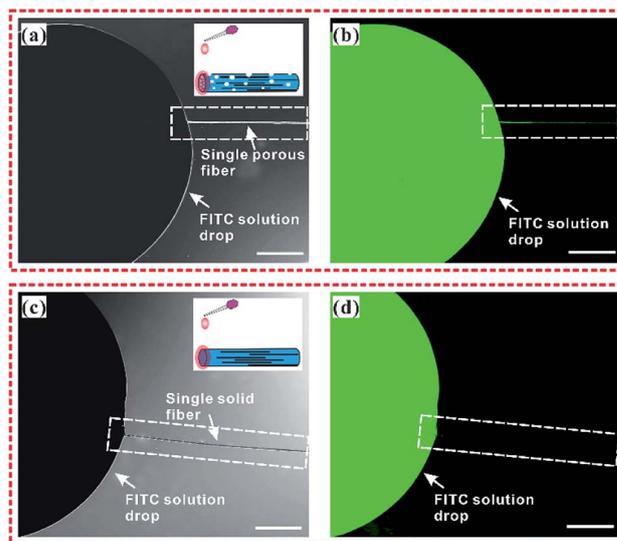

Fig. 6 The transport of FITC/ethanol solution in one single Ag NWs/PS composite fiber. The optical microscope images (a and c) and corresponding fluorescence microscope images (b and d) of FITC/ethanol solution transport in the porous and solid Ag NWs/PS composite fibers. (a and b) is porous fiber; (c and d) is solid fiber. Inset is the schematic illustration of the experimental process. The scale bar is 50 μm.

NWs/PS porous fiber mats because 4-ATP has distinct Raman features. Another very important reason for choosing 4-ATP as probe molecule is that it can be used as a Raman active molecule by attaching onto Ag NWs, and this structure is then used to capture and detect the target biomolecules through their specific binding sites,[39,40] which means we can anchor the 4-ATP molecule onto our prepared SERS substrates as a linker to capture and detect some biomolecules in our follow-up study.[41] To prepare the SERS substrates, large-sized electrospun fiber mats were cut into strips (1.0 × 0.5 cm²) firstly, and then these strips were immersed into 4-ATP/methanol solutions with different concentrations for only 10 seconds. Finally, these infiltrated strips were taken out quickly and dried in a culture dish naturally at ambient temperature prior to the measurement. When the substrate was immersed into the 4-ATP/ethanol solution, the probe molecule can permeate the fiber quickly and access the surface of Ag NWs efficiently because of the large amount of holes. Fig. 7a shows a set of SERS spectra for 0.1 M 4-ATP adsorbed on the Ag NWs/PS porous fibers with different Ag NW contents. It is obvious that the higher the content of Ag NWs in the PS fiber, the higher the intensity of the Raman signal. When more Ag NWs are embedded in the fiber, the spacing between adjacent nanowires is smaller, which can generate more electromagnetic fields for adsorbed 4-ATP molecules and result in the Raman signal enhancement.[20,35] Six characteristic 4-ATP peaks can be seen at 1077, 1147, 1175, 1396, 1446, and 1573 cm⁻¹ when the Ag NW content was 50 mg. Three intense vibrational bands are found around the wavenumbers of 1077, 1175, and 1573 cm⁻¹, which arise from the C–S stretching, C–H bending and C–C stretching modes of 4-ATP, respectively.[42–45] The bands at 1396 and 1446 cm⁻¹ are assigned to the N=N stretching vibrations of 4,4′-
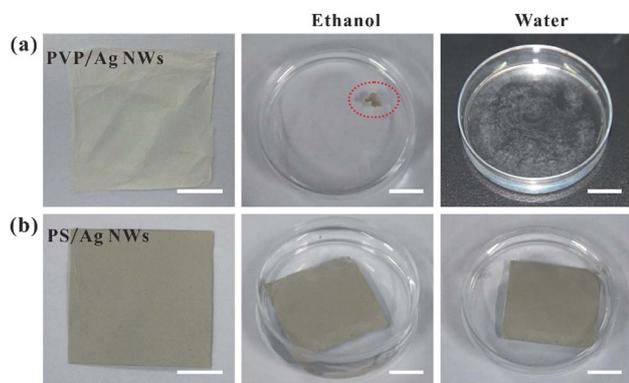

Fig. 5 Photographs of (a) 10 mg-Ag NWs/PVP and (b) 50 mg-AgNWs/PS electrospun fiber mats before and after immersion in ethanol or water. All scale bars are 1 cm.
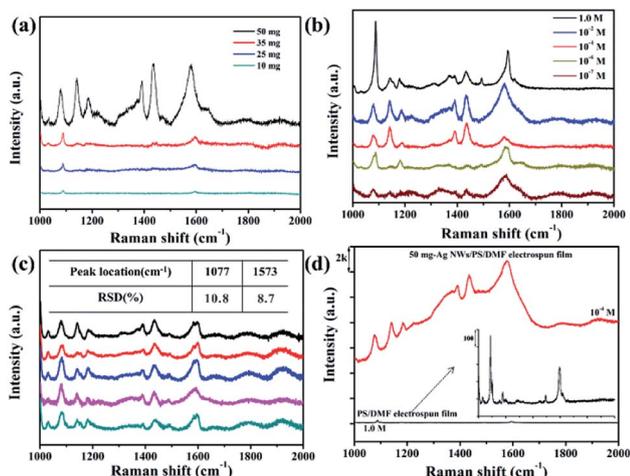
Fig. 7 (a) SERS spectra of 0.1 M 4-ATP adsorbed on the Ag NWs/PS porous fibers with different Ag NW contents; (b) SERS spectra of different 4-ATP concentrations (1.0 M, 10^{-2} M, 10^{-4} M, 10^{-6} M and 10^{-7} M) adsorbed on the 50 mg-Ag NWs/PS porous fibers; (c) SERS spectra of 10^{-4} M 4-ATP recorded from five different regions of the 50 mg-Ag NWs/PS fibers; (d) Raman spectra of 10^{-4} M 4-ATP adsorbed on the 50 mg-Ag NWs/PS porous fibers and pure PS porous fibers without Ag NWs.

dimercaptoazo-benzene (DMAB), which are generated from the interactions between two adjacent 4-ATP molecules.[39] When the content of Ag NWs is lower than 50 mg, only the 1077 and 1573 cm^{-1} vibration peaks are identical and become weaker and weaker. Therefore, the electrospun mats obtained from 50 mg-Ag NWs/PS/DMF solution were used as SERS substrate in subsequent experiments.

Fig. 7b shows the SERS spectra of different 4-ATP concentrations (1.0 M, 10^{-2} M, 10^{-4} M, 10^{-6} M and 10^{-7} M) adsorbed on the 50 mg-Ag NWs/PS porous fibers. As the concentration of probe molecule becomes lower and lower, the number of detected peaks becomes less and less, and the peak values are weaker and weaker. However, the wavenumbers of 1077 and 1573 cm^{-1} still could be detected clearly, but the width of these bands became wider. We suppose this unusual phenomenon is caused by the fluorescence enhancement effect, implying a non-distinct Raman property.[46] Herein, the electrospun SERS substrate was able to detect 4-ATP at a low concentration of 10^{-7} M. The reproducibility of Raman signals for the Ag NWs/PS substrate was evaluated by collecting the SERS spectra of 4-ATP molecules from 5 randomly selected positions on the same strip. As shown in Fig. 7c, the number of peaks and their wavenumbers were almost the same, which demonstrated good reproducibility of the SERS signals. Relative standard deviation (RSD) is always used to evaluate the quality of reproducibility. The RSD indicating reproducibility of signal intensity has been calculated and is shown in the inset of Fig. 7c. The SERS peaks basically locate at 1047 and 1573 cm^{-1}, and their intensity RSD are 10.8% and 8.7%, respectively.

Fig. 7d shows the Raman spectra of 10^{-4} M 4-ATP adsorbed on the 50 mg-Ag NWs/PS porous fibers and pure PS porous fibers without Ag NWs. It is obvious that the signal intensity of the

Raman spectrum is greatly enhanced by the addition of Ag NWs. The enhancement factor (EF) was calculated by using the following equation:[47] EF = $(I_{SERS}/I_{non\text{-}SERS}) \times (C_{non\text{-}SERS}/C_{SERS})$, where I_{SERS} and $I_{non\text{-}SERS}$ are the intensities of the SERS and the non-SERS signal of the peak in consideration, respectively, and C_{SERS} and $C_{non\text{-}SERS}$ are the concentrations of the target molecule on the SERS and non-SERS surfaces, respectively. The EF was $\sim 10^5$ for the case of 4-APT when calculated using the peak at 1573 cm^{-1}.

In order to highlight the advantage of the prepared Ag NWs/PS porous fibers in terms of sample collection efficiency, the SERS spectra of 10^{-4} M 4-ATP adsorbed on different substrates (including electrospun porous/solid fibers and casted porous/solid films) with same collection time were measured as shown in Fig. 8. For comparability, the content of Ag NWs in all substrates is the same at 50 mg, and the concentration of 4-ATP is 10^{-4} M. All the substrates were cut into small strips of the same area, and then immersed into 4-ATP solution for the same amount of time (only 10 seconds). Finally, these infiltrated strips were taken out and dried at room temperature for SERS measurements. As expected, 4-ATP molecules adsorbed on the porous fibers show the strongest Raman signal (Fig. 8a), and the intensity of the peak at 1573 cm^{-1} was up to 1.3×10^4. This is mainly because the large number of pores can adsorb more 4-ATP solution in a unit of time, which leads to more 4-ATP molecules adsorbed on the surface of Ag NWs. For comparison, 4-ATP molecules adsorbed in the solid fibers show very weak Raman signal, as shown in curve 4 of Fig. 8a, and the intensity of the peak at 1573 cm^{-1} was only 286. There are two main reasons for the weak Raman signal of 4-ATP adsorbed in solid fibers. On the one hand, the adsorption capacity of solid fibers for 4-ATP solution is small, resulting in less 4-ATP molecules adsorbed on its surface; on the other hand, Ag NWs were embedded into PS fibers, and the encapsulated polymer can prevent the 4-ATP molecule access to the surface of Ag NWs. There are similar phenomena in the casted films, and the SERS spectra of 4-ATP molecules adsorbed on porous film (Fig. S9a†) and solid film (Fig. S9b†) are shown in curves 2 and 3 in Fig. 8a, with the intensity of the peak at 1573 cm^{-1} being 3272 and 627, respectively. The large amount of holes in the fibers greatly improve the sample collection efficiency of the SERS-active substrate and facilitate the adsorption of analyte on the surface of Ag NWs.
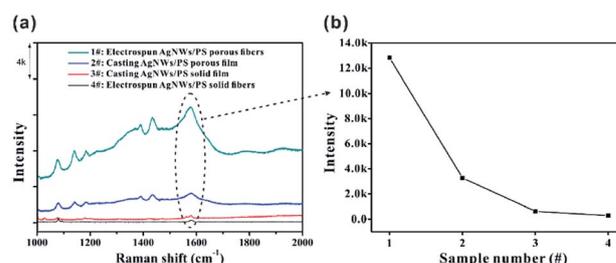

Fig. 8 (a) SERS spectra of 10^{-4} M 4-ATP collected on different substrates; (b) peak intensity of 1573 cm^{-1} in different SERS spectra in (a).

4. Conclusions

In summary, we have successfully fabricated a novel SERS-active substrate assembled by Ag NW-embedded porous PS fibers *via* electrospinning. Ag NWs are embedded in porous PS fiber and aligned orderly along the axis direction. The large amounts of holes in the fibers greatly improve the sample collection efficiency of the SERS-active substrate and facilitate the adsorption of analyte on the surface of Ag NWs. The as-prepared electrospun mats were successfully applied as SERS substrates in the analysis of 4-ATP. The detection limit for 4-ATP of our 50 mg Ag NWs/PS fiber mat is 10^{-7} M, and the electrospun fiber mats have shown good detection reproducibility of SERS signals. The produced flexible and free-standing SERS substrates may have potential application in wearable sensors for the trace detection of chemical and biological molecules.

Conflicts of interest

There are no conflicts to declare.

Acknowledgements

References

1 M. Fleischman, P. J. Hendra and A. J. McQuillan, *Chem. Phys. Lett.*, 1974, **26**, 163.

2 D. L. Jeanmaire and R. P. Van Duyne, *J. Electroanal. Chem.*, 1977, **84**, 1.

3 T. Yang, L. Zhan and C. Z. Huang, *Trends Anal. Chem.*, 2020, **124**, 115813.

4 M. E. Farrell, E. L. Holthoff and P. M. Pellegrino, *Proc. SPIE*, 2012, **8358**, 835816.

5 S. Bettini, S. Pal, S. Sawalha, A. Licciulli, L. Valli, G. Giancane and R. Pagano, *ChemistrySelec*, 2019, **4**, 2968.

6 K. Xu, R. Zhou, K. Takei and M. Hong, *Adv. Sci.*, 2019, 1900925.

7 Y.-C. Liu, C.-C. Yu and S.-F. Sheu, *J. Mater. Chem.*, 2006, **16**, 3546.

8 R. A. Tripp, R. A. Dluhy and Y. Zhao, *Nanotoday*, 2008, **3**, 31.

9 X. Tan, J. Melkersson, S. Wu, L. Wang and J. Zhang, *ChemPhysChem*, 2016, **17**, 2630.

10 Y. Lee, J. Lee, T. K. Lee, J. Park, M. Ha, S. K. Kwak and H. Ko, *ACS Appl. Mater. Interfaces*, 2015, **7**, 26421.

11 Z. Fan, R. Kanchanapally and P. C. Ray, *J. Phys. Chem. Lett.*, 2013, **4**, 3813.

12 M. Gen and C. K. Chan, *Atmos. Chem. Phys.*, 2017, **17**, 14025.

13 M. Gen, R. Kunihisa, A. Matsuki and C. K. Chan, *Aerosol Sci. Technol.*, 2019, **53**, 760.

14 S. M. Restaino and I. M. White, *Anal. Chim. Acta*, 2019, **1060**, 17.

15 E. S. Prikhozhdenko, D. N. Bratashov, D. A. Gorin and A. M. Yashchenok, *Nano Res.*, 2018, **11**, 4468.

16 D. He, B. Hu, Q.-F. Yao, K. Wang and S.-H. Yu, *ACS Nano*, 2009, **3**, 3993.

17 C. Chen, Y. Tang, B. Vlahovic and F. Yan, *Nanoscale Res. Lett.*, 2017, **12**, 451.

18 J. Xue, T. Wu, Y. Dai and Y. Xia, *Chem. Rev.*, 2019, **119**(8), 5298.

19 C.-L. Zhang, K.-P. Lv, H.-P. Cong and S.-H. Yu, *Small*, 2012, **8**, 648.

20 C.-L. Zhang, K.-P. Lv, N.-Y. Hu, Yu Le, X.-F. Ren, S.-L. Liu and S.-H. Yu, *Small*, 2012, **8**, 2936.

21 Z. C. Liu, Z. D. Yan, L. Jia, P. Song, L. Y. Mei, L. Bai and Y. Q. Liu, *Appl. Surf. Sci.*, 2017, **403**, 29.

22 J. Shi, T. You, Y. Gao, X. Liang, C. Li and P. Yin, *RSC Adv.*, 2017, **7**, 47373.

23 L. Zhang, X. Gong, Y. Bao, Y. Zhao, M. Xi, C. Jiang and H. Fong, *Langmuir*, 2012, **28**, 14433.

24 J. Shao, L. Tong, S. Tang, Z. Guo, H. Zhang, P. Li, H. Wang, C. Du and X.-F. Yu, *ACS Appl. Mater. Interfaces*, 2015, **7**, 5391.

25 Z. Liu, Z. Yana and L. Bai, *New J. Chem.*, 2018, **42**, 11185.

26 M. Fan, G. F. S. Andrade and A. G. Brolo, *Anal. Chim. Acta*, 2020, **1097**, 1.

27 J. Li, W. Zhang, Q. Li and B. Li, *Nanoscale*, 2015, **7**, 2889.

28 W. Yuan, P. Y. Gu, C. J. Lu, K. Q. Zhang, Q. F. Xu and J. M. Lu, *RSC Adv.*, 2014, **4**, 17255.

29 P. Dayal, J. Liu, S. Kumar and T. Kyu, *Macromolecules*, 2007, **40**, 7689.

30 J. Lin, B. Ding, J. Yang, J. Yu and G. Sun, *Nanoscale*, 2012, **4**, 176.

31 C.-L. Zhang, K.-P. Lv, H.-T. Huang, H.-P. Cong and S.-H. Yu, *Nanoscale*, 2012, **4**, 5348.

32 W. Yuan and K.-Q. Zhang, *Langmuir*, 2012, **28**, 15418.

33 C. Wu, W. Yuan, S. S. Al-Deyabb and K.-Q. Zhang, *Appl. Surf. Sci.*, 2014, **313**, 389.

34 W. Yuan, N. Zhou, L. Shi and K.-Q. Zhang, *ACS Appl. Mater. Interfaces*, 2015, **7**, 14064.

35 F. J. García-Vidal and J. B. Pendry, *Phys. Rev. Lett.*, 1996, **77**, 1163.

36 Y. Badra and M. A. Mahmoud, *Spectrochim. Acta, Part A*, 2006, **63**, 639.

37 Y. Sun and Y. Xia, *Analyst*, 2003, **128**, 686.

38 G. Zhu and D. Chen, *J. Mater. Sci.: Mater. Electron.*, 2012, **23**, 2035.

39 L. Kang, P. Xu, D. Chen, B. Zhang, Y. Du, X. Han, Q. Li and H.-L. Wang, *J. Phys. Chem. C*, 2013, **117**, 10007.

40 Z. Deng, P. Wen, N. Wang and B. Peng, *Sens. Actuators, B*, 2019, **288**, 460.

41 L. Xu, W. Yan, W. Ma, H. Kuang, X. Wu, L. Liu, Y. Zhao, L. Wang and C. Xu, *Adv. Mater.*, 2015, **27**, 1706.

42 A. Philip, B. Ankudze and T. T. Pakkanen, *Appl. Surf. Sci.*, 2019, **480**, 229.

43 B. Ankudze, A. Philip, T. T. Pakkanen, A. Matikainen and P. Vahimaa, *Appl. Surf. Sci.*, 2016, **387**, 595.

44 B. Cao, B. Liu and J. Yang, *CrystEngComm*, 2013, **15**, 5735.

45 X. Hu, T. Wang, L. Wang and S. Dong, *J. Phys. Chem. C*, 2007, **111**, 6962.

46 D. A. Weitz and S. Garoff, *J. Chem. Phys.*, 1983, **78**, 5324.

47 K. Jalaja, S. Bhuvaneswari, M. Ganiga, R. Divyamol, S. Anup, J. Cyriac and B. K. George, *Anal. Methods*, 2017, **9**, 3998.